Journal of Experimental Botany, Vol. 72, No. 18 pp. 6474–6489, 2021
doi:10.1093/jxb/erab255 Advance Access Publication 3 June 2021

RESEARCH PAPER

Detection of the metabolic response to drought stress using hyperspectral reflectance

Angela C. Burnett*, Shawn P. Serbin, Kenneth J. Davidson, Kim S. Ely and Alistair Rogers

Environmental and Climate Sciences Department, Brookhaven National Laboratory, Upton, NY, USA

* Correspondence: acb219@cam.ac.uk

Received 3 March 2021; Editorial decision 28 May 2021; Accepted 2 June 2021

Editor: Ros Gleadow, Monash University, Australia

Abstract

Drought is the most important limitation on crop yield. Understanding and detecting drought stress in crops is vital for improving water use efficiency through effective breeding and management. Leaf reflectance spectroscopy offers a rapid, non-destructive alternative to traditional techniques for measuring plant traits involved in a drought response. We measured drought stress in six glasshouse-grown agronomic species using physiological, biochemical, and spectral data. In contrast to physiological traits, leaf metabolite concentrations revealed drought stress before it was visible to the naked eye. We used full-spectrum leaf reflectance data to predict metabolite concentrations using partial least-squares regression, with validation R^2 values of 0.49–0.87. We show for the first time that spectroscopy may be used for the quantitative estimation of proline and abscisic acid, demonstrating the first use of hyperspectral data to detect a phytohormone. We used linear discriminant analysis and partial least squares discriminant analysis to differentiate between watered plants and those subjected to drought based on measured traits (accuracy: 71%) and raw spectral data (66%). Finally, we validated our glasshouse-developed models in an independent field trial. We demonstrate that spectroscopy can detect drought stress via underlying biochemical changes, before visual differences occur, representing a powerful advance for measuring limitations on yield.

Keywords: Abscisic acid (ABA), climate change, crop breeding and management, drought stress, leaf reflectance, metabolites, remote sensing, stress responses, water deficit, water stress.

Introduction

Water is vital for life. For much of the planet, climate change is creating a hotter, drier world, impacting plant productivity across both managed and unmanaged ecosystems (Franklin *et al.*, 2016). Agricultural irrigation alone is responsible for two-thirds of our freshwater withdrawals (Poore and Nemecek, 2018), and the provision of water for agriculture is threatened by acute and chronic water shortages. These shortages are driven by increased drought—water shortage caused by low rainfall—and heightened demand for water for other purposes; both drivers will increase during the coming century (Cattivelli *et al.*, 2008; http://www.fao.org/land-water/land/en/). At the same time, a significant increase in crop yield is required to feed the growing global population (Ort *et al.*, 2015; FAO, 2018; Simkin *et al.*, 2019). We therefore urgently need

high-yielding crops with high water use efficiency, in addition to improved water management practices, in order to sustain future crop production (Morison *et al.*, 2008; Leakey *et al.*, 2019).

There are a number of plant traits indicative of a drought response. It is well known that plants respond to drought in myriad ways, underpinned by a suite of genetic, biochemical, and physiological adjustments and adaptations (Chaves *et al.*, 2009; Fàbregas and Fernie, 2019). These responses are orchestrated by signalling pathways, mediated in particular by the phytohormone abscisic acid (ABA) (Sreenivasulu *et al.*, 2012; Munemasa *et al.*, 2015; Sah *et al.*, 2016; Zhu, 2016). ABA levels increase dramatically in drought-stressed leaves, and ABA regulates almost 10% of protein-coding genes as well as inducing many genes involved in carbohydrate metabolism (Sreenivasulu *et al.*, 2012; Thalmann and Santelia, 2017). Physiologically, ABA decreases stomatal conductance in order to reduce water loss via transpiration, and this, together with reduced rates of photosynthesis, is a key indicator of drought stress (Chaves *et al.*, 2009). Biochemically, species differ in their responses to drought but typically show an early increase in the content of leaf sugars, which can act as osmotic protectors (Thalmann and Santelia, 2017), followed by an increase in ABA and amino acids, including the important osmotic protector proline (Fàbregas and Fernie, 2019).

Characterizing the drought stress responses of plants is essential for understanding the effects of drought, and the interactions of these effects with key life processes such as growth and reproduction. This is critical for developing effective tools for crop breeding and management in the face of reduced water supply, for example the capacity to screen different crop varieties for drought stress tolerance in order to select parents for breeding. Traditional techniques for measuring drought stress are extremely robust, yet can be costly and time-consuming. Remote sensing techniques offer a novel solution to improve the speed of detection for small- and large-scale applications (AghaKouchak *et al.*, 2015). The physiological and metabolic profile of a drought-stressed plant is traditionally captured with measurements of photosynthetic parameters using gas exchange and fluorescence, and biochemical measurements following destructive leaf harvesting. Physiological breeding (Reynolds and Langridge, 2016) involves the consideration of physiological traits, including those related to water use efficiency, in crop breeding systems (Leakey *et al.*, 2019). This increases the efficacy of breeding for abiotic stress resilience, yet lengthy measurements reduce throughput. Physiological breeding would be greatly enhanced by remote sensing techniques which deliver high-throughput, non-destructive, and relatively low-cost estimates of critical physiological and biochemical plant traits for crop breeding and management using passive optical and thermal imaging techniques *inter alia* (Serbin *et al.*, 2012, 2014, 2015; Couture *et al.*, 2016; Yendrek *et al.*, 2017; Silva-Perez *et al.*, 2018; Ely *et al.*, 2019; Meacham-Hensold *et al.*, 2019; Shiklomanov *et al.*, 2019). In particular, the use of high spectral resolution spectroscopic reflectance data—the collection of numerous contiguous reflected wavelengths—to predict drought phenotypes is of great value for crop breeders screening for improved water use efficiency and drought stress tolerance, and for farmers managing water supply for maximal yield in a changing environment. Crucially, quantifying drought stress before it can be detected visually—by identifying plants in the pre-drought condition using spectroscopy to detect known leaf-level metabolic changes caused by drought stress—would provide a major advance in drought prediction and mitigation.

Spectral data can predict a range of biochemical and physiological traits, with several key advances using partial least-squares regression (PLSR) to predict diverse traits of interest in recent years. For example, models to predict maximum carboxylation capacity of Rubisco and electron transport rate have been developed in aspen and cottonwood (Serbin *et al.*, 2012), maize (Yendrek *et al.*, 2017), wheat (Silva-Perez *et al.*, 2018), tobacco (Meacham-Hensold *et al.*, 2019), and crop canopies (Serbin *et al.*, 2015). Prediction of a range of leaf structural and biochemical traits has also been achieved, such as leaf mass per unit area (LMA) in a range of tree species (Serbin *et al.*, 2014), secondary metabolites such as tannins in birch and aspen (Couture *et al.*, 2016), chlorophyll in maize (Yendrek *et al.*, 2017), and a suite of metabolites including protein, starch, amino acids, and several sugars in a range of agronomic species (Ely *et al.*, 2019). PLSR involves the building of a statistical relationship between spectroscopic data and measured traits. Subsequently, leaf traits may be predicted using these spectroscopic or 'hyperspectral' data alone. Spectral data have also been used to examine drought stress in plants, but traditionally this has been performed using two-band spectral vegetation indices (SVIs) such as the normalized difference vegetation index (NDVI), photochemical reflectance index (PRI), and water band index (WBI) which are known to correlate with water stress and associated changes such as a change in pigment pools (Zarco-Tejada *et al.*, 2012, 2013; Rossini *et al.*, 2013; Ballester *et al.*, 2018; Gerhards *et al.*, 2019). However, these indices do not provide a mechanistic explanation: they do not reveal the metabolic and physiological processes underpinning the drought response. Furthermore, indices often do not show good generality between species and experiments (e.g. Rapaport *et al.*, 2017).

Our approach moves beyond the use of indices correlated with drought, to detect specific metabolic signals linked to the mechanisms underpinning the drought response, using hyperspectral leaf reflectance data. We sought to use full-spectrum hyperspectral data, which is a more powerful and comprehensive measurement than an index using only two wavebands from within the spectrum, to predict the metabolic changes underpinning the drought response before it is visible to the naked eye in order to develop a rapid yet comprehensive picture of drought stress which is lacking

when indices are used. Secondly, in addition to predicting changes in metabolites for which it has already been demonstrated that prediction is possible using hyperspectral data, we sought to use hyperspectral data to predict the concentrations of ABA and proline, which are two key metabolites in the drought response for which no relationship with hyperspectral data has yet been developed. Indeed, to our knowledge, no phytohormone has yet been predicted from hyperspectral data, and this would greatly improve the prospects of using hyperspectral data for plant stress detection since phytohormones are frequently involved in stress signalling upstream of (and therefore earlier than) metabolic changes. Finally, we wished to examine the applicability of our approach by scaling up from the glasshouse environment to an independent field trial, carried out the following year.

In our glasshouse experiment, we imposed drought (a full dry-down treatment) on a diverse range of agronomic species and utilized physiological, biochemical, and spectroscopic techniques to characterize the drought response. Rather than simulate a realistic, ephemeral drought stress using careful water monitoring, our aim was to generate a strong drought response in all species, thus the full dry-down method was selected (Fàbregas and Fernie, 2019). We hypothesized that spectroscopy could be used to quantitatively detect the critical indicators which are known to underpin the metabolic response to drought stress, including drought-induced changes in ABA and proline concentrations, as well as carbohydrates, for the purposes of rapid and early identification of drought. To date, ABA and proline have not been predicted from spectral data, and this would provide a major advance to the field. Our overarching goal was to elicit a drought response and evaluate our ability to detect signals of drought stress using spectroscopy. Specifically, we addressed the following research questions. (i) Can metabolic signals be used to predict drought stress before drought is visible to the naked eye? (ii) Can spectroscopy be used to detect these key metabolic signals? (iii) Can spectroscopy be used to identify drought stress before signs of drought are detected visually?

Materials and methods

Plant material and growth conditions for the glasshouse experiment

A range of agronomic species with differing morphological and physiological characteristics were selected, to maximize trait variation. As well as considering a range of characteristics to maximize trait variation, species were also selected based on the following two criteria. Firstly, each species has leaves that can readily be measured using a spectroradiometer; that is, large enough to obtain quality measurements without the need for joining many samples together in a 'raft'. Secondly, each species is readily grown in the Long Island region so that our findings are relevant for the local agricultural environment and to facilitate our subsequent field study which focused on one species of particular interest (*Cucurbita pepo*) identified from the results of the glasshouse study in order to validate our findings. Seeds of *Capsicum annuum* var. Sweet Chocolate (bell pepper), *C. pepo* L. var. Costata Romanesco (courgette), *Helianthus annuus* var. Pro Cut Gold F1 (sunflower), and *Raphanus sativus* var. Easter Egg (radish) were all obtained from Johnny's Selected Seeds, Winslow, ME, USA. *Setaria italica* (foxtail millet) and *Sorghum bicolor* (sorghum, mixed colours broomcorn) seeds were obtained, respectively, from Deer Creek Seed, Windsor, WI, USA and Seed Savers, Decorah, IA, USA. *Populus×canadensis* clone OP367 (hybrid poplar) cuttings were obtained from Cold Stream Farm, Free Soil, MI, USA. Plants were grown in the glasshouse at Brookhaven National Laboratory, Upton, NY, USA in spring and summer 2018 under a 14 h photoperiod and temperatures of 17–33 °C:17–29 °C day:night. Plants were grown under ambient light conditions with supplementary lighting of 49 W m^{-2} provided by high-pressure sodium bulbs. The maximum light level was 2078 μmol m^{-2} s^{-1} photosynthetic photon flux density (PPFD). The maximum relative humidity was 99%. Environmental conditions were recorded by a weather station located in the glasshouse. The station was comprised of a humidity and temperature sensor (ATMOS 14, METER Group, Inc., Pullman, WA, USA) and two quantum sensors (QSO S and PYR, Apogee Instruments, Logan, UT, USA). Seeds were sown in BM2 germinating mix (Berger, Saint-Modeste, Quebec, Canada), and seedlings were subsequently transplanted to 30 litre pots filled with Pro-Mix BX Mycorrhizae growing medium (Premier Tech Horticulture, Quakertown, PA, USA). Poplar cuttings were soaked in water until roots developed, then grown in 100 litre pots filled with 52 Mix (Conrad Fafard, Inc., Agawam, MA, USA). Plants were watered three times per week, with the exception of plants undergoing the drought treatment. Pots were raised to provide an air gap between the base of the pot and the glasshouse floor and to prevent root exploration and water uptake from the glasshouse floor during the drought treatment. Osmocote Plus slow-release fertilizer (The Scotts Company, Marysville, OH, USA) was added according to the manufacturer's instructions, and pesticides were applied at fortnightly intervals in accordance with usage directions. Due to a low sample size, *S. italica* was omitted from the detailed species-level analysis but was included in the modelling approaches to maximize trait diversity and increase robustness.

Drought treatment and measurement schedule for glasshouse-grown plants

Plants were randomly assigned to either the drought or the control treatment, with 50% of the plants of each species allocated to each treatment and distributed randomly. Water was completely withheld from droughted plants, from the onset of the drought treatment until the end of the experiment, with the first day of missed watering being designated day 0 of the drought treatment; control plants received water three times per week. For each species, the experiment ended when leaves were fully desiccated; that is, meaningful gas exchange, metabolic, or spectral data could no longer be collected. Final measurements were made for each species as follows: after 35 d of drought for *C. annuum*, after 32 d for *C. pepo*, after 29 d for *H. annuus*, after 37 d for *P. canadensis*, after 33 d for *R. sativus*, and after 23 d for *S. bicolor*. During the drought treatment, soil moisture content was measured daily at 16.00 h (HS2-12 soil-water sensor, Campbell Scientific, Logan, UT, USA). The 20 cm probe was used for 100 litre pots and the 12 cm probe was used for 30 litre pots. Spectral and gas exchange measurements were performed between 08.30 h and 13.30 h at regular intervals throughout the treatment. Leaf harvesting was carried out between 11.30 h and 14.30 h, always paired with collection of spectral data. For the main (glasshouse) experiment, n=12 plants per treatment for *C. annuum* and *C. pepo*, and n=8 plants per treatment for *H. annuus*, *R. sativus*, *P. canadensis*, and *S. bicolor*. At each time point in the experiment, one leaf was removed from each individual and then discs were removed as described below. Each individual oven-dried or flash-frozen sample was a pool of multiple discs from the same individual leaf, such that there were either 12 or eight samples taken for each treatment at each time point (depending on

the species) representing true biological units (one sample per plant, with the experimental treatment applied at the plant level). At each time point throughout the measurement period, a different leaf was harvested from the same individuals. Spectral data were collected on more dates than harvests were carried out, due to the destructive nature of leaf sampling. All measurements were performed on the newest fully expanded leaf. The leaf plastochron index (LPI) system (Erickson and Michelini, 1957) was used to track leaf development over time in *P. canadensis*. Measurements of *P. canadensis* focused on the leaf at position LPI 11, where LPI 0 was the first leaf to be at least 25 mm long.

Visual assessment of drought

Plants were regularly photographed and the images visually assessed to establish the date on which a drought effect was first visible for each species in the aboveground part of the plant. To avoid bias, this visual assessment was carried out in isolation once all photographs had been collected, and prior to all analyses of the physiological, biochemical, and spectral data including any analysis of the number of days taken for drought signals to be identified using those techniques. Visible signs of drought varied between species (Fig. 1). In the first instance, visible signs were: wilting including a change in leaf angle in *C. annuum*, yellowing and wilting in *C. pepo*, wilting including a change in leaf angle in *H. annuus*, yellowing of the lower leaves in *P. canadensis*, wilting in *R. sativus*, and wilting including a change in leaf angle in *S. bicolor* (Fig. 1; Supplementary Fig. S1).

Gas exchange

Survey-style gas exchange measurements were performed as described previously (Burnett *et al.*, 2019), for three species, using four LI-6400XT Portable Photosynthesis Systems, each with a Leaf Chamber Fluorometer (LI-COR, Lincoln, NE, USA), zeroed using a common nitrogen standard. Measurements were taken following a brief (<2 min) stabilization period in the leaf cuvette. The reference CO_2 concentration was 400 μmol mol^{-1}. Saturating irradiances used for gas exchange measurements were determined for each species using light response curves: 1500 μmol photons m^{-2} s^{-1} for *R. sativus*; 1800 μmol photons m^{-2} s^{-1} for *H. annuus* and *S. bicolor*. The flow rate was 200–500 μmol s^{-1}. Block temperature was set to ambient. Gas exchange data in the manuscript are presented in accordance with the data standard published by Ely *et al.* (2021). Raw gas exchange data are available in Dataset at EcoSIS (https://doi.org/10.21232/UTK8zaW4).

Leaf traits

Leaf samples were harvested using a metal punch of known area and were either immediately flash-frozen in liquid nitrogen for biochemical analysis, or oven-dried for elemental carbon and nitrogen analysis (oven-dried samples comprised a separate batch of material taken from the same leaf used for the flash-frozen samples). The selection of the leaf punch depended on the size of the leaf being harvested, and ranged from 0.95 cm^2 to 3.46 cm^2; multiple discs were harvested for each sample and the total area calculated. Discs were taken from across the area of the leaf in order to account for the variation within a leaf. Leaf metabolic traits were then expressed on an area basis (see Dataset at EcoSIS https://doi.org/10.21232/UTK8zaW4). For each assay, samples were randomized prior to analysis. Analysis of elemental carbon and nitrogen on ground oven-dried samples was performed as described previously (Burnett *et al.*, 2016). Sufficient material was available to provide three aliquots of the frozen ground homogenized material of each sample (i.e. of the material from each harvested leaf). One aliquot of frozen material underwent ethanol extraction, followed by analysis of a suite of carbon- and nitrogen-containing metabolites (Burnett *et al.*, 2016,

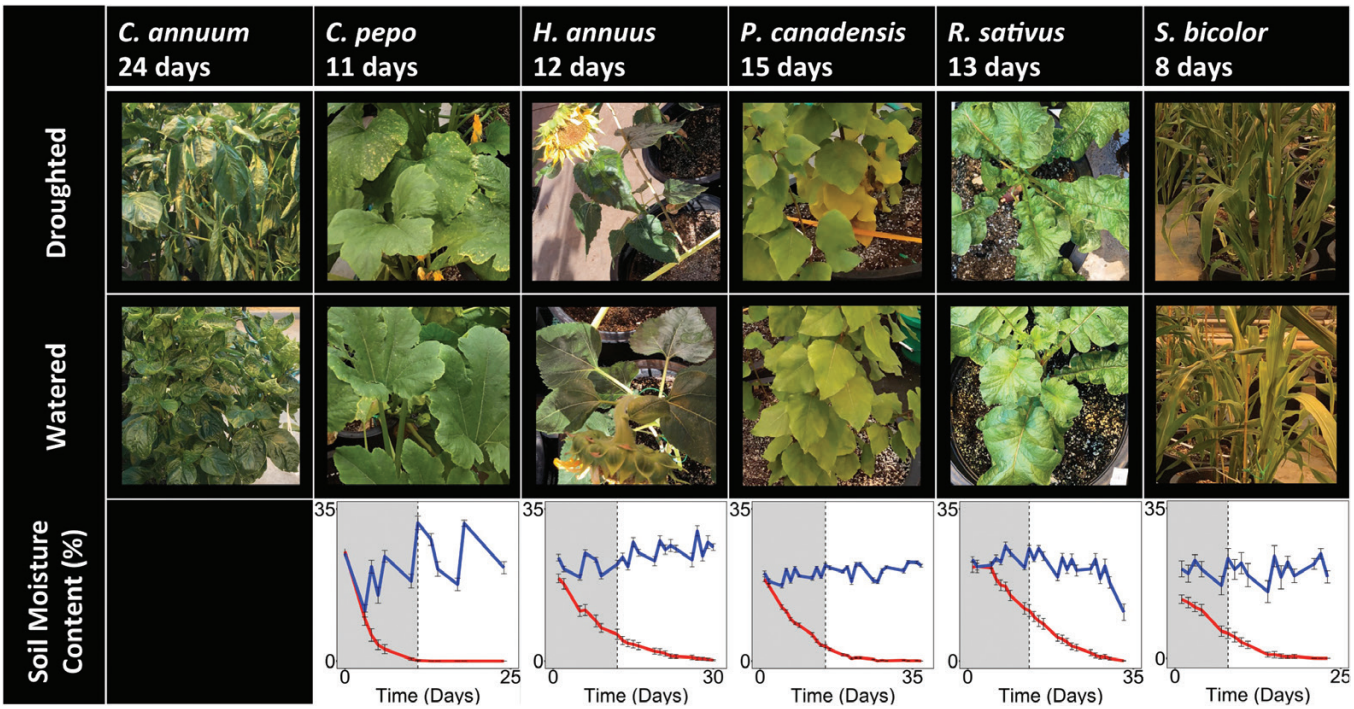

Fig. 1. First visible differences between drought-treated and watered plants. Photographs show drought-treated and watered plants of each species on the first day when drought could be visually detected (identified in the top row). Soil moisture content is shown for watered (blue) and drought-treated (red) plants of each species, with SEs about the mean (n=12 plants per treatment for *C. pepo*; n=8 plants per treatment for *H. annuus*, *R. sativus*, *P. canadensis*, and *S. bicolor*). The grey portion of each plot shows the time period before drought could be detected visually. No soil moisture data are available for *C. annuum*.

2018), including fructans for monocot species. A second aliquot of frozen leaf material was used for the ABA assay. Samples were placed in 500 µl of ABA extraction buffer per 33 mg sample and incubated overnight on a shaker (4 °C, 180 rpm, in the dark). ABA extraction buffer contained 80% methanol (v/v in H_2O), 100 mg l^{-1} butylated hydroxytoluene dissolved in methanol, and 500 mg l^{-1} citric acid dissolved in H_2O. ABA assays were performed using Phytodetek assay kits utilizing the competitive antibody binding method (Agdia, Elkhart, IN, USA) following an established method (Kim *et al.*, 2012). The protocol was recovery-tested prior to use, and ABA concentrations were determined using a standard curve. A third aliquot of frozen leaf material was used for the proline assay. Proline assays were performed following sample extraction in sulfosalicylic acid, acidic ninhydrin, and toluene (Sunkar, 2010); total free proline concentrations were determined using a standard curve. For every assay, two technical replicates were run for the material from each leaf and the results averaged to give one value per leaf sample.

Leaf water content (LWC) was measured using the following equation:

$$\mathrm{LWC}\,(\,\%\,) = \frac{(\text{leaf fresh mass} - \text{leaf dry mass})}{\text{leaf fresh mass}} \times 100$$

Leaf trait data, including metabolic traits and LWC, are available in Dataset at EcoSIS https://doi.org/10.21232/UTK8zaW4.

Spectroscopy

Leaf spectral reflectance data were collected using a PSR+ full-range (continuous 350–2500 nm) spectroradiometer (Spectral Evolution, Lawrence, MA, USA) connected to a leaf clip assembly with an internal, calibrated light source (SVC, Poughkeepsie, NY, USA). The spectroradiometer was calibrated using a LabSphere Spectralon® reflectance standard (LabSphere, Inc., North Sutton, NH, USA). Three to four spectra were collected from across the adaxial surface of each leaf and averaged to give a single spectrum for each leaf at each time point. Leaf temperature was measured immediately prior to each spectral measurement using an infrared radiometer (Apogee Instruments, Logan, UT, USA). Spectral data collection was performed according to established procedures (Serbin *et al.*, 2012; Ely *et al.*, 2019). Spectral data are available in Dataset at EcoSIS https://doi.org/10.21232/UTK8zaW4.

Field-grown C. pepo used for validation of the approach

Seeds of *C. pepo* L. var. Dunja were obtained from the Long Island Cauliflower Association (Riverhead, NY, USA) and sown in twelve 10 m×10 m plots, surrounded by a *C. pepo* border the same width as 1.5 times the height of the mature vegetation, and sown at a density to achieve full canopy coverage, in a research field at Brookhaven National Laboratory in 2019. Following germination and establishment, irrigation was maintained at standard local agricultural levels for watered plants (six plots), and withheld for plants subjected to drought (six plots). Biochemical and spectral data were collected on these plants as described above, within 3 h of solar noon, with n=3 reps per plot on each measurement day. Each replicate of leaf material was composed of a set of leaf discs punched from across the area of the leaf and pooled to make one sample from one leaf, thus material from three plants per plot was harvested on each measurement day. Since the experimental treatment was applied at the plot level, the three plants per plot represent pseudoreplicates, with n=6 plots subjected to drought and n=6 watered plots measured on each day. Due to the abundance of plant material, different plants within each plot were measured on each measurement day. Each leaf was harvested immediately following spectral data collection.

Data analysis

Data analysis was performed in the R open source software environment (R Core Team, 2019). For statistical analysis of physiological traits, an overall linear mixed-effects model was first fit for each trait for each species in turn, testing for effects of (and interactions between) treatment categories and time into the drought experiment, keeping the individual plant as a random effect. Subsequently, to examine differences between watered and droughted plants at individual time points, repeated-measures ANOVA was performed for each trait for each species to account for the repeated nature of the measurements performed on individual plants outlined above. Then, estimated marginal means were calculated and a post-hoc Tukey test was performed to identify non-cumulative, pairwise differences between drought-treated and watered plants at each individual time point. For statistical analysis of leaf biochemical traits (measured using traditional approaches), an initial linear mixed-effects model was first fit for all data for each trait to test for effects of (and interactions between) the fixed effects of species, treatment, and time into the drought experiment, keeping the individual plant as a random effect. Then, a repeated-measures ANOVA with a post-hoc Tukey test was performed for each species and each trait, to compare each time point, as described above. When required, data were log-transformed prior to analysis to provide normality.

We developed relationships between spectral data and leaf traits measured on an area basis using a PLSR modelling approach. PLSR was performed using the 'pls' package (Mevik and Wehrens, 2007) in R, following methods developed previously (Serbin *et al.*, 2014; Ely *et al.*, 2019). PLSR models perform best when a wide range of trait values are used to build the model (i.e. the use of a large 'trait space'), in order to establish strong predictive power within that range of values (Schweiger, 2020). For this reason, for all metabolites in this study, except ABA, data from all species were pooled for model training and testing. For ABA, the PLSR model using the full-species dataset only yielded an R^2 value of 0.09; thus it was decided to build an ABA PLSR model using data from *C. pepo* only, which yielded a much higher R^2.

For PLSR model building, spectral wavelengths of 500–2400 nm were used for all trait predictions with the exception of starch and the *C. pepo*-only model for ABA. In these two cases, the range 1100–2400 nm was used to improve the accuracy of prediction. For two models, proline and the *C. pepo*-only model for ABA, spectral data were transformed prior to analysis, using $\log_{10}(1/\text{reflectance})$, to improve model fit. When appropriate, leaf trait data were $\log_{10}$- or square-root-transformed in order to produce a normal distribution prior to PLSR as detailed in Table 1, and a small number of samples were rejected from the dataset due to outlier residual errors in order to develop a model reflecting the trait space covered by the majority of data points. Observational data points were subset according to species then randomly assigned to calibration and validation datasets composed of 80% and 20% of the data, respectively. Component selection and model calibration were carried out as described previously (Serbin *et al.*, 2014; Ely *et al.*, 2019). The R^2 and root mean square error (RMSE) of prediction of the validation dataset were used to assess each model. The variable importance of projection (VIP) was used for qualitative evaluation of model predictor variables (Wold *et al.*, 2001). For the application of glasshouse-built PLSR models to novel spectra collected on field-grown *C. pepo*, glasshouse-derived model coefficients were applied to field spectra for trait prediction. For a tutorial guide on using the PLSR method please see Burnett *et al.*, 2021.

Discriminant analyses were used to identify the ability to statistically separate control and drought treatment classes in our datasets. Linear discriminant analysis (LDA) was for use with our measured or predicted trait data, and partial least squares discriminant analysis (PLS-DA) was for use with spectral data. The LDA model built with glasshouse data used a 75:25 calibration/training and model validation/testing split of the data stratified according to treatment; model training was performed with leave-one-out calibration. Receiver operator curve (ROC) optimization of the number of components was performed; ROC analysis and the standard area under the curve (AUC) value indicating model accuracy of prediction for the glasshouse LDA model are presented in Supplementary Fig. S2. LDA models for field data were built with leave-one-out calibration, and were based on the suite of traits established and

Table 1. Data used to prepare partial least-squares regression (PLSR) models presented in Fig. 5.

PLSR model	Cal	Val	nComps	Data transformation	Spectra transformation
Nitrogen	382	97	12	Square-root	–
Starch	343	87	13	Square-root	1100–2400 nm only
Protein	397	105	8	–	–
ABA	67	17	8	Log_{10}	$Log_{10}(1/R)$ 1100–2400 nm only
Amino acids	347	92	10	Square-root	-
Proline	348	90	11	Square-root	$Log_{10}(1/R)$

'Cal' and 'Val' indicate the number of data points allocated to the calibration (training) and validation (testing) dataset for each PLSR model presented in Fig. 5 (plots in Fig. 5 show the validation data). 'nComps' indicates the number of components used in each PLSR model. 'Data transformation' indicates transformations performed on biochemical data prior to model building in order to achieve a normal distribution. 'Spectra transformation' indicates when spectral wavebands were transformed as $log_{10}(1/R)$ where R is reflectance, in order to improve model fit; this column also indicates that for starch and ABA, wavebands in the restricted range 1100–2400 nm, rather than the full range 500–2400 nm, were selected to minimize noise.

Table 2. Prediction of plant drought from spectral data using partial least squares discriminant analysis (PLS-DA).

Spectral data used in PLS-DA model	Validation accuracy	Kappa value	No. of spectra in training dataset	No. of spectra in testing dataset	No. of components
Glasshouse data identified in the first column were divided for model training and model testing					
All glasshouse spectra	66%	0.3224	1316	438	21
First temporal quartile of glasshouse spectra	59%	0.1847	312	103	13
Second temporal quartile of glasshouse spectra	60%	0.2037	328	108	9
Third temporal quartile of glasshouse spectra	68%	0.3692	394	130	17
Fourth temporal quartile of glasshouse spectra	94%	0.8716	285	94	21
All glasshouse data were used for model training; field data were used for model testing					
All glasshouse spectra, testing all field spectra	63%	0.2578	1754	321	21
All glasshouse spectra, testing first temporal half of field spectra	71%	0.4199	1754	180	21
All glasshouse spectra, testing second temporal half of field spectra	53%	0.0455	1754	141	21
All glasshouse spectra, testing first 10 d of field spectra	70%	0.4	1754	70	21

The upper portion of the table shows the results of models trained and tested using glasshouse spectra; the lower portion shows the results of models trained using glasshouse spectra and tested using spectra measured on field-grown *C. pepo*. The percentage accuracy of the model for the validation (testing) dataset, validation kappa accuracy, number of spectra used to train and test the model, and number of model components selected, are presented. AUC values and ROC analyses are given in Supplementary Fig. S3.

validated for the glasshouse models, taking into account the effectiveness of trait prediction in the field.

PLS-DA models built for the main (glasshouse) dataset also used a 75:25 split of the data for model training and model testing, with 10-fold cross-validated resampling repeated five times on the training data, and ROC optimization of the number of components. ROC analysis and AUC values are presented in Supplementary Fig. S3. PLS-DA models ran for up to 100 iterations, until convergence was reached. When PLS-DA models were applied to spectral data for field-grown *C. pepo*, the split of model training (glasshouse) and testing (field) data deviated from 75:25, as detailed in Table 2. In each case, the full glasshouse dataset was used for model calibration, with field data used as a validation of model performance in the outdoor setting. For the full-species models for metabolite data, PLS-DA, PLSR, and LDA, *S. italica* data were included in order to increase the trait variation and therefore the predictive capability of the models; *S. italica* was excluded from species-level metabolite plots due to low sample size. PLS-DA was performed using the 'caret' package (Kuhn, 2008) in R, as described previously (Cotrozzi and Couture, 2020; Gold *et al.*, 2020). For our PLS-DA models, we also report the number of components used for each permutation of the data (Table 2). The number of components is an essential attribute, and is sometimes provided (Cavender-Bares *et al.*, 2016; Fallon *et al.*, 2020), yet many other past studies have often omitted to report the associated number of PLS-DA components (e.g. Susič *et al.*, 2018; Zovko *et al.*, 2019). We openly report our data and encourage other authors to do the same to facilitate more fair comparisons of overall model performance.

Results

Physiological measurements only reveal drought after visual drought detection

Visual detection of drought occurred on different days for the six different species in the main study, ranging from 8 d to 24 d into the treatment (Fig. 1; Supplementary Fig. S1). Gas exchange measurements were performed for three species and revealed a significant and marked decrease in net CO_2 exchange per leaf area (A) and stomatal conductance to water vapour per leaf area (g_{sw}) in drought-treated compared with watered plants of each species (Fig. 2). *Helianthus*

annuus (Fig. 2A, D) maintained higher rates of A and g_{sw} throughout drought when compared with *S. bicolor* (Fig. 2C, F) in which we observed near-zero rates of A and g_{sw} at the end of the drought treatment. This is consistent with the idea that *H. annuus* is anisohydric, meaning that it maintains water use and A during drought at the possible cost of hydraulic failure, while *S. bicolor* is known to be isohydric, limiting g_{sw} as a method of reducing risk of hydraulic failure while reducing A and risking carbon starvation. Differences between A and g_{sw} in watered and drought-treated *H. annuus* occurred later into the drought treatment and were of proportionally smaller magnitude than the effect observed in *S. bicolor* (Fig. 2A, C, D, F). Notably, the decrease in A and g_{sw} always occurred after visual detection of drought in each species (Fig. 2). Therefore, for the species we investigated here, traditional measurements of leaf gas exchange are inadequate for early detection of drought stress since changes in photosynthesis and stomatal conductance only manifested after visible drought effects were observed.

Biochemistry reveals pre-visual metabolic indicators of drought

The metabolic profile of each species varied greatly, with different sets of metabolites indicating a response to drought stress (Fig. 3). Broadly speaking, the drought indicators ABA and proline increased during drought along with elemental leaf nitrogen, protein, and total free amino acids, whilst starch decreased (see Fig. 3 legend). In addition to the different metabolic profiles, the magnitude of the drought stress response varied greatly between species, with *C. pepo* and *P. canadensis* showing the greatest percentage of metabolic changes between drought-treatred and watered plants. Thirdly, the timing of the response differed between species, with pre-visual changes in metabolite levels occurring in four of the six species. These pre-visual changes were strongest in *C. annuum* and *C. pepo*: each showed a sustained change in one or more metabolites prior to visual drought detection (Fig. 4). 'Sustained' indicates that the change was significant from its onset until the end of the drought experiment.

The key pre-visual, sustained indicator of drought stress was ABA in both *C. annuum* and *C. pepo*, accompanied by starch in *C. annuum*. In *C. annuum*, starch decreased ($P<0.05$ at 21 d into drought treatment, subsequently $P<0.001$; the increase at the first two time points was non-significant) and ABA increased throughout the drought treatment, significant from 21 d into drought treatment onwards ($P<0.05$, subsequently $P<0.01$; the magnitude of the relative difference varied over time). For both starch and ABA, the first significant differences were detected 3 d before visual detection of drought in *C. annuum*. In *C. pepo*, a significant increase in ABA ($P<0.01$, subsequently $P<0.001$) was detected from 6 d into the drought

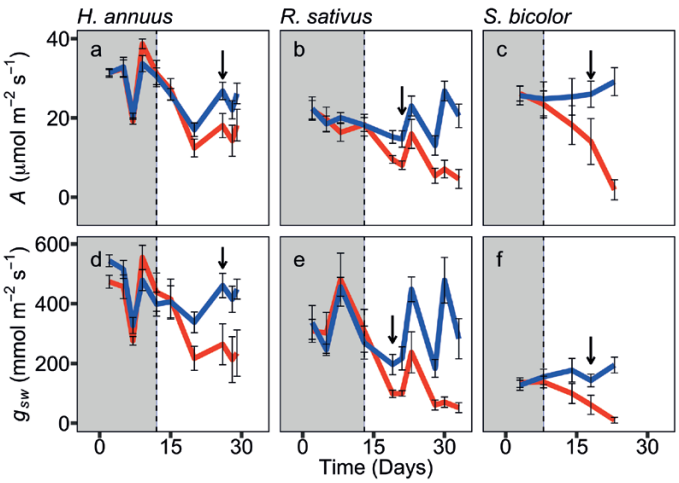

Fig. 2. Photosynthesis and stomatal conductance only decrease after drought stress is visible to the naked eye. Panels show net CO_2 exchange per leaf area (A, *H. annuus*; B, *R. sativus*; C, *S. bicolor*) and stomatal conductance to water vapour per leaf area (D, *H. annuus*; E, *R. sativus*; F, *S. bicolor*). Blue lines denote watered plants; red lines denote drought-treaed plants. Bars show 1 SE above and below the mean (n=8 plants per treatment for each species). The grey portion of each plot shows the time period before drought could be detected visually. Black arrows indicate the day on which the first statistically significant difference in A or g_{sw} was detected between drought-treated and watered plants. A model including all time points revealed highly significant interactions between time and treatment for A and g_{sw}, for each species as follows. For *H. annuus*, $F=14.0_{(1,138)}$, $P<0.001$ for A; $F=29.8_{(1,138)}$, $P<0.001$ for g_{sw}. For *R. sativus*, $F=44.3_{(1,142)}$, $P<0.001$ for A; $F=52.4_{(1,142)}$, $P<0.001$ for g_{sw}. For *S. bicolor*, $F=28.0_{(1,58)}$, $P<0.001$ for A; $F=37.3_{(1,58)}$, $P<0.001$ for g_{sw}. Pairwise post-hoc comparisons revealed the following differences. *Helianthus annuus* showed a significant decrease in A and g_{sw} from 26 d into drought, sustained until the end of measurement (on days 26, 28, 29: for A $P<0.05$, df 63, 63, 66.4; for g_{sw} $P<0.01$, df 55.3, 55.3, 56.2; A, D). *Raphanus sativus* showed a significant sustained decrease in A from day 21 onwards ($P<0.05$ on days 21, 23, 28; $P<0.001$ on days 30, 33; df 128) and a significant sustained decrease in g_{sw} from day 19 ($P<0.05$ on days 19, 21; $P<0.001$ on days 23, 28, 30, 33; df 110; B, E). *Sorghum bicolor* showed a significant sustained decrease in A and g_{sw} from day 18 of drought (for A on day 18 $P<0.05$, on day 23 $P<0.001$, df 48.9; for g_{sw} on day 18 $P<0.05$, on day 23 $P<0.001$, df 57.1; C, F).

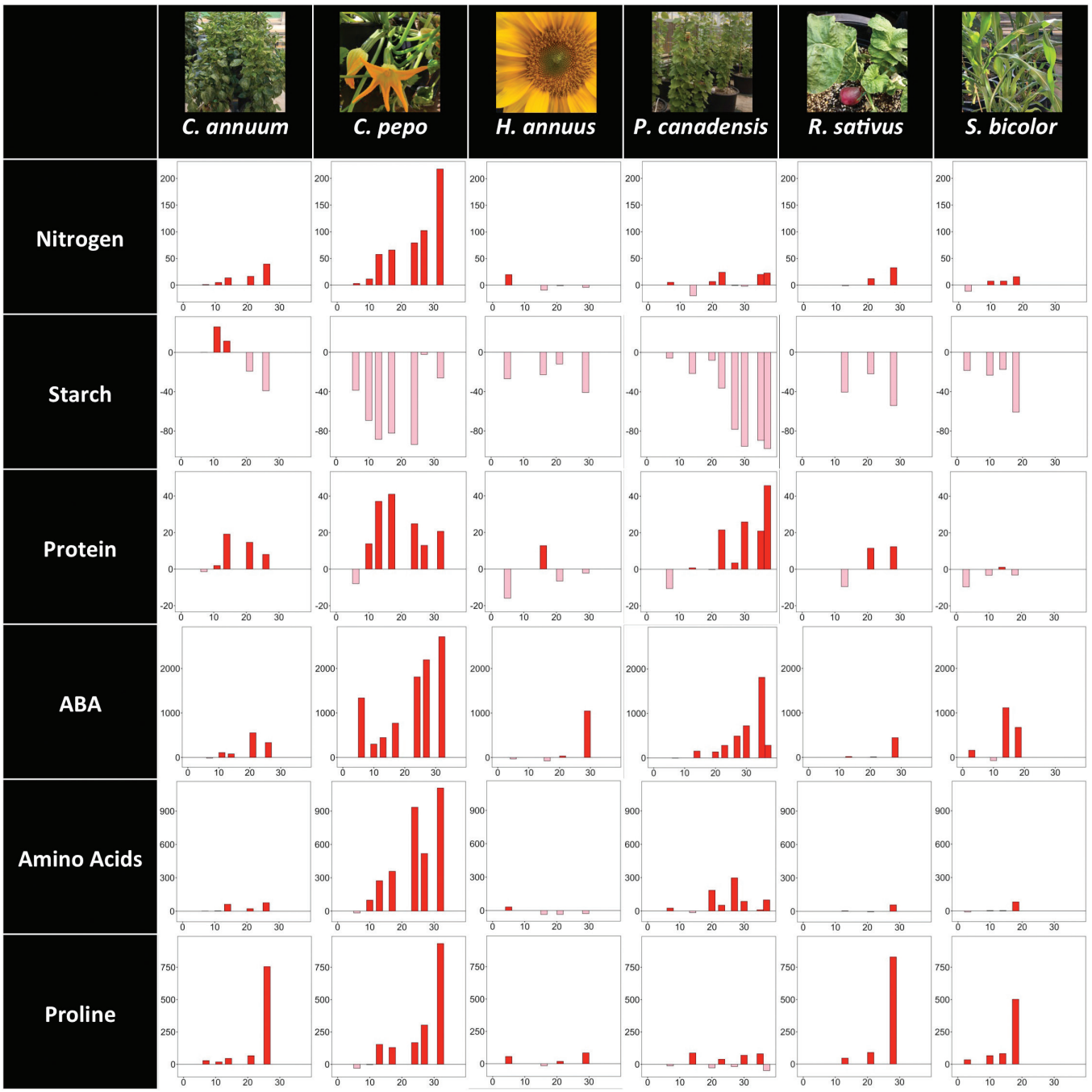

Fig. 3. The metabolic response to drought varies between species. For key metabolites affected by the drought treatment, percentage changes in droughted relative to watered plants are shown for each species. Red bars indicate an increase in the level of a metabolite under drought treatment; pink bars indicate a decrease under drought treatment. In each case, the *x*-axis displays days into the drought treatment (with the same axis limits used for all plots) and the *y*-axis displays percentage change (*y*-axis limits are constant across all species but are adjusted for each metabolite as follows: nitrogen –20% to +220%; starch –100% to +25%; protein –20% to +50%; ABA –100% to +2700%; amino acids –50% to +1100%; proline –50% to +950%). The horizontal black line indicates no change. For each time point, represented by an individual bar, n=12 plants per treatment for *C. annuum* and *C. pepo*; n=8 plants per treatment for *H. annuus*, *R. sativus*, *P. canadensis*, and *S. bicolor*. The traits presented here were selected from a suite of biochemical analyses (see the Materials and methods) using a linear model including all species and all biochemical traits, which identified the following overall changes during drought: nitrogen P<0.05; amino acids P<0.01; proline P<0.01; starch P<0.001; ABA P<0.001. Protein did not show a significant drought response in the overall model but is included here due to its role as an early metabolic indicator of drought in *C. annuum* and *C. pepo* (Fig. 4).

treatment, providing an early indication of drought 5 d before visual detection. The relative difference in ABA between watered and drought-treated plants persisted throughout the experiment, with an initial spike followed by differences of steadily increasing magnitude as time progressed. In addition to these sustained changes, both *C. annuum* and *C. pepo* displayed

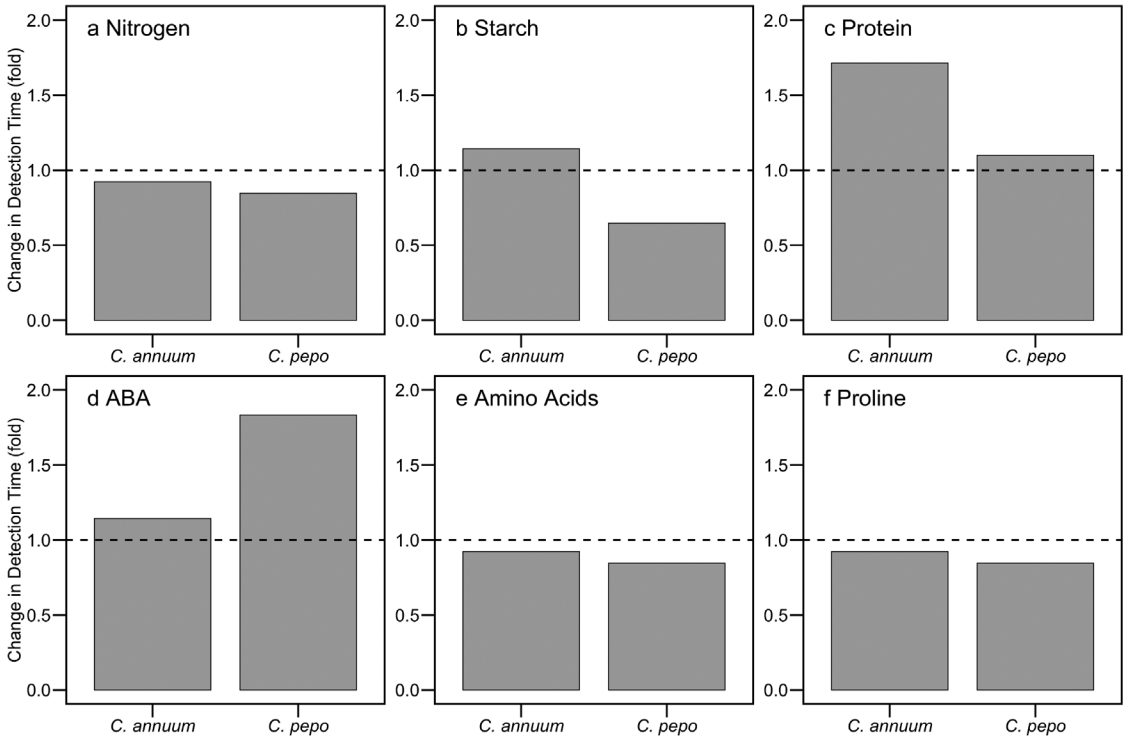

Fig. 4. Metabolic signals can indicate drought before it is visible in *C. annuum* and *C. pepo*. Out of six key metabolites, three (starch, protein, and ABA) are able to improve drought detection time in *C. annuum* and/or *C. pepo* when compared with visual detection, with starch and ABA signals sustained throughout drought. Metabolites shown are (A) nitrogen, (B) starch, (C) protein, (D) ABA, (E) amino acids, and (F) proline. The dashed horizontal line represents no change; bars above the dashed line are faster than visual detection whilst bars below the dashed line are slower than visual detection. Detection time was identified as the first time point with a significant trait difference between drought-treated and watered plants in each case; n=12 plants per treatment for each species.

an unsustained but pre-visual significant increase in protein (P<0.05 in each case; the initial decrease in protein seen in Fig. 3 was non-significant for both species). Finally, *H. annuus* displayed a short-term pre-visual increase in nitrogen (P<0.05), while *P. canadensis* displayed an unsustained pre-visual change in total non-structural carbohydrates (the sum of glucose, fructose, sucrose, and starch) and glucose (P<0.05 in each case).

Later in the drought treatment, once drought was already visible to the naked eye, we observed a significant difference in each of the six metabolites for *C. annuum* and *C. pepo*, as characterized in Fig. 3. Considering these six metabolites, in *H. annuus* a significant difference was observed for nitrogen, ABA, and amino acids; in *P. canadensis* for starch, protein, ABA, and amino acids; in *R. sativus* for all six metabolites except protein; and in *S. bicolor* for starch, ABA, amino acids, and proline. Thus, ABA accumulates in plants of all species subjected to drought, and proline accumulates in drought-treated plants of *C. annuum*, *C. pepo*, *R. sativus*, and *S. bicolor.* Due to the large changes observed in drought-treated plants for each trait (Fig. 3), we next hypothesized that the combination of these six metabolites would be sufficient to predict the droughted condition of plants, due to additive effects of small non-significant pre-visual changes combining with significant effects to enable early detection of drought in all species.

LWC was maintained until late into the drought treatment, and did not show a statistically significant change until after the time at which drought could be detected with the naked eye, in each species studied. In *C. annuum*, LWC did not change in drought-treated plants until the final time point, 2 d after drought was detected with the naked eye. At this time, LWC was lower in drought-treated plants (P<0.001). In *C. pepo*, LWC showed a significant difference (P<0.01) 27 d into the drought treatment, which was 16 d after drought was visible to the naked eye, yet there was no difference in LWC in subsequent measurements. In *H. annuum*, LWC never showed a significant difference between drought-treated and watered plants. Plants of *P. canadensis* showed a significant difference (P<0.05) in LWC 15 d after drought was visibly detectable, but, as observed for *C. pepo*, this difference did not persist in later measurements. *Raphanus sativus* plants showed a decrease (P<0.001) in LWC in drought-treated plants at the final time point, 15 d after visual detection of drought. Finally, *S. bicolor* showed a decrease in LWC (P<0.05, increasing to P<0.001) in drought-trated plants, starting 6 d after visual detection of drought.

Linear discriminant analysis allows prediction of drought from key metabolites

We performed an LDA with measured values of the six key leaf traits associated with the observed drought response: nitrogen, starch, protein, ABA, amino acids, and proline. Data were separated for model building (n=401) and model validation (n=133). The success of prediction of the class 'droughted' or 'watered' for the validation dataset, averaged across 10 iterations, was 71% (±4% SD), with a kappa value of 0.42 (±0.08 SD) and an AUC of 0.77 (±0.04 SD; see Supplementary Fig. S2). With reference to the overall model including all time points, success of prediction increased when progressively later time points were selected and earlier time points excluded, since drought effects were more pronounced towards the end of the experiment, making classification easier.

We have demonstrated that the robust approach of measuring metabolites using traditional biochemical techniques facilitates early detection of drought stress (research question i), shown by analysing individual traits and developing an all-species LDA model for drought prediction. However, the destructive nature of these measurements and the relatively time-consuming process of laboratory analysis are two major disadvantages of using this technique for rapid detection of drought stress in the breeding or production environment. Therefore, we next examined whether spectroscopy could be used to characterize the drought-related metabolic profiles of plants (ii), and whether this technique could also be used for pre-visual detection of drought stress (iii).

Spectroscopy enables rapid accurate prediction of leaf metabolites

PLSR models were used to build relationships between observed leaf traits derived from traditional biochemical techniques, and traits predicted using spectroscopic data (Fig. 5). Spectroscopic data are both non-destructive and quick to collect, overcoming the two disadvantages associated with collecting and analysing biochemical data identified above. Independent validation of PLSR for key drought-related traits reveals a strong capacity for the prediction of nitrogen, starch, protein, ABA, amino acids, and proline (Fig. 5). For the first time we developed relationships between biochemically observed and spectrally predicted values of ABA and proline with validation R^2 values of 0.50 and 0.84, respectively (Fig. 5D, F). This suggests that it may be possible to use spectral data to estimate these key drought indicators non-destructively.

Spectroscopy enables early detection of drought

Having demonstrated the use of metabolic drought signals to detect drought pre-visually using biochemical analysis, and used spectral data to reveal those signals rapidly and non-destructively utilizing PLSR models, we turned to our third question: can spectroscopy be used to identify drought stress before visual detection? We evaluated two approaches: the use of PLS-DA to interrogate the spectral data directly, and the use of PLSR to predict traits that were then used to detect drought stress using a standard LDA approach. Each approach was developed and tested using glasshouse data. Finally, the applicability and robustness of each approach was tested by independent validation using spectra collected from a separate drought experiment conducted in the field.

PLS-DA enables accurate drought classification from spectral data

Firstly, PLS-DA was used to determine the treatment class of leaf samples ('droughted' or 'watered') using full-range spectra from all data points in the study with an overall validation accuracy of 66% (Table 2). When all-species data were divided temporally into quartiles, classification accuracy increased with each successive quartile due to the increasing severity of the treatment (Table 2). To test the robustness of this diagnostic approach, PLS-DA models built using the data from the main experiment performed in the glasshouse were applied to spectra measured on *C. pepo* grown in the field in a separate drought experiment (Table 2). When the main all-species dataset was used as the PLS-DA model training data, with novel field-grown *C. pepo* data as the testing data, the success of 'droughted' or 'watered' class prediction for field-grown *C. pepo* was 63%. When the testing data were composed of field-grown *C. pepo* spectra from only the second half of the drought treatment period rather than the entire period, overall model accuracy decreased to 53% (Table 2) due to mitigation of the drought treatment by rainfall events. However, when the testing data were composed of only the field-grown *C. pepo* spectra from the first half of the drought treatment period rather than the entire period, the model predicted the class of field-grown *C. pepo* with 71% accuracy (Table 2), indicating good detection of the onset of drought stress in the field—the most critical time for stress detection.

Predicted traits derived from spectra enable accurate classification of drought

Secondly, PLSR-derived predicted traits were used to examine the possibility of detecting the 'droughted' or 'watered' class. PLSR models developed from the main experiment (Fig. 5) were applied to spectra collected from the independent field-grown *C. pepo* to generate predictions of the key metabolites identified in Fig. 3. The predicted values of each trait obtained using these glasshouse PLSR models were then validated against observed metabolite data from the field experiment (Fig. 6). Extrapolating models from the glasshouse to the field is notoriously difficult because glasshouse- and field-grown plants have different leaf structures due to varying abiotic and biotic conditions (Poorter *et al.*, 2012, 2016). Despite these

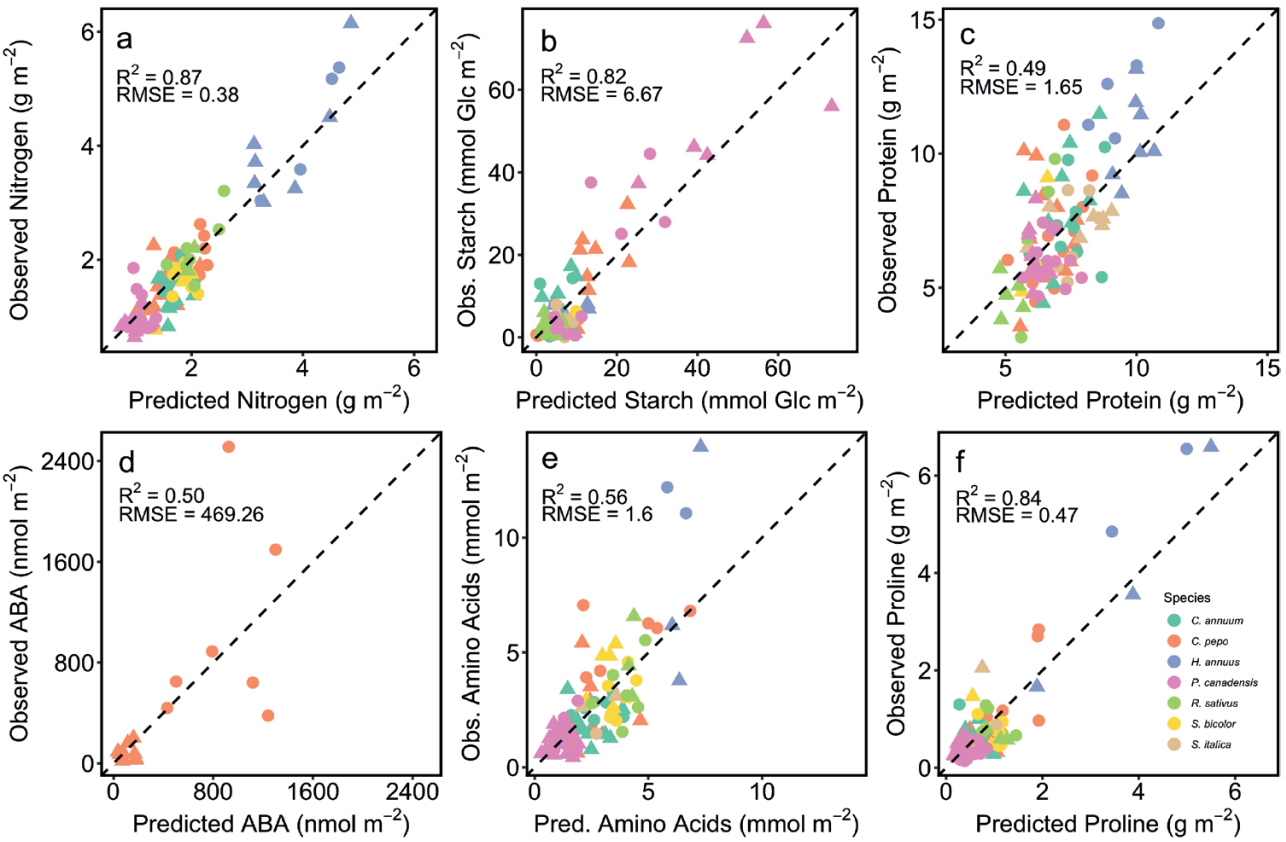

Fig. 5. Partial least-squares regression predicts values of five key metabolites. Model validation plots show the relationship between observed metabolite concentrations (measured using traditional techniques) and predicted concentrations obtained using partial least-squares regression (PLSR) performed for (A) nitrogen, (B) starch, (C) protein, (D) ABA, (E) amino acids, and (F) proline. Circles indicate drought-treated plants; triangles indicate watered plants; points are coloured according to the species key in (F). All plots show original, untransformed data. Each model was built using a calibration dataset and tested using a validation dataset; plots show validation data. Details of the datasets are provided in Table 1. Note that for ABA, only data from *C. pepo* were used for the development of a PLSR model (see the Materials and methods).

challenges, trait prediction was successful for both starch and protein (Fig. 6A, B), and moderate for ABA and amino acids (Fig. 6C, D). When applying our glasshouse models to the field, however, trait prediction for proline was unsuccessful (Fig. 6E). The effective estimation of proline from spectral data in the glasshouse (Fig. 5f) indicates that this metabolite is especially sensitive to issues of model tuning between the glasshouse and field. We expect that re-tuning models with field data would yield a more widely applicable model.

LDA was performed using predicted trait values for starch, protein, ABA, nitrogen, and amino acids, obtained from PLSR modelling performed on field spectra. These predicted traits showed moderate success at predicting the 'droughted' or 'watered' class of *C. pepo* field samples with 63% accuracy (n=321). When the five observed field traits (observed starch, protein, ABA, amino acids, and proline) obtained from biochemical measurement of field samples were used in LDA, the accuracy was 67% (n=182). When predicted field traits for only the first 10 d of the drought treatment were used in LDA, class prediction accuracy was 74% (n=70). Thus, the predicted traits achieved a moderate level of class prediction accuracy exceeding the prediction accuracy of observed traits. This is likely to be due to marked qualitative differences in the magnitude of traits between drought-treated and watered plants; that is, a qualitative 'low' or 'high' trait value may be predicted using PLSR even whilst the quantitative predicted trait value deviates from the observed value; the error in the PLSR models is normal, meaning that additional bias is not introduced. The class prediction accuracy from predicted traits was highest (74%) during the first 10 d of the drought treatment in the field, indicating its potential for early detection of drought stress.

Discussion

Traditional approaches used to quantify the impacts of drought stress on crop physiology include measurements of gas exchange and fluorescence. While providing detailed information, these measurements are often slow and laborious, limiting their

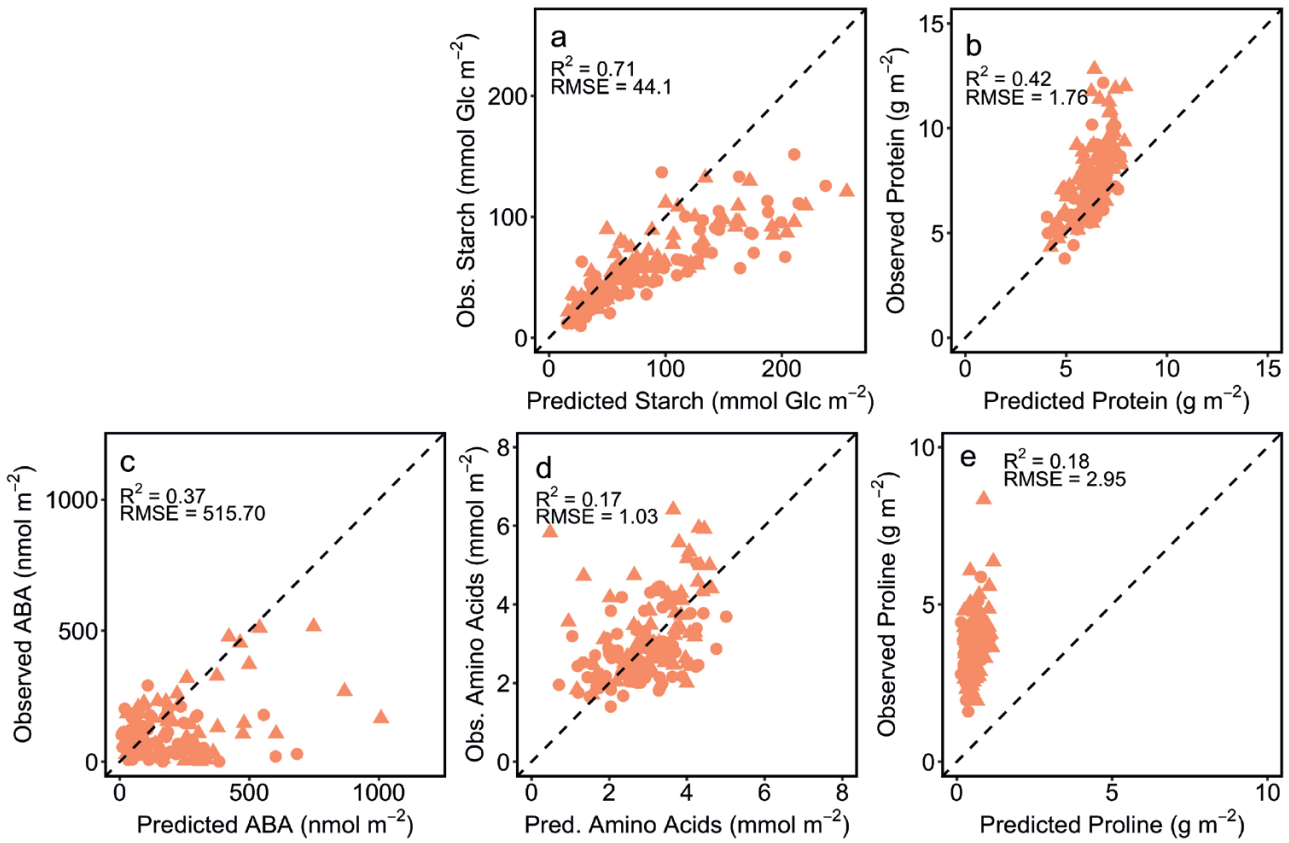

Fig. 6. Models built using glasshouse data predict leaf metabolite concentrations from spectra in watered and drought-treated field-grown *C. pepo*. Partial least-squares regression (PLSR) model coefficients were applied to novel spectra measured on field-grown *C. pepo* (*n*=321) and used to predict the following key metabolites: (A) starch, (B) protein, (C) ABA, (D) amino acids, and (E) proline. Prediction was validated with observed metabolite concentrations for field-grown *C. pepo* and was successful for starch and protein. Circles indicate drought-treated plants; triangles indicate watered plants. Models used were the same as those described in Fig. 5, and the same data transformations were performed (Table 1). All plots show untransformed data. Nitrogen data are not available for field-grown *C. pepo*.

utility for field trials and rapid phenotyping (Rapaport *et al.*, 2017; Burnett *et al.*, 2019). Furthermore, as we have shown here, metabolic changes occur in advance of physiological changes, and these key signals are even more difficult to analyse in real-time and require destructive harvesting, preventing their effective use in crop management. New approaches that can enable rapid non-destructive monitoring of crop status are critically needed to advance plant breeding for the production of food, fuel, and fibre in a future production environment where drought stress will be more common. Integrating different methods will be important to enable the necessary advances (Cattivelli *et al.*, 2008). Spectroscopy has already been successfully used to predict biochemical and physiological traits in crop plants (Yendrek *et al.*, 2017; Silva-Perez *et al.*, 2018). Here we have demonstrated that leaf metabolic indicators can be used to predict drought stress before it is visible to the naked eye (research question i), that reflectance spectroscopy can be used to detect these key metabolic indicators of drought (ii), and that this technique can be used to detect drought before it becomes visually apparent (iii). We have shown for the first time that ABA and proline—two crucial players in the drought response—can be predicted from leaf reflectance spectroscopy. We have also shown, for the first time, that spectroscopy can be used to predict drought stress via detection of the underlying metabolic changes. Taken together, these novel results highlight the use of spectroscopy as a valuable approach yielding new, high-throughput, metabolite-focused tools for crop breeding and management.

High-throughput phenotyping is a vital part of crop breeding (Claeys and Inzé, 2013; Araus *et al.*, 2018), and remote sensing will make an important contribution (Araus and Cairns, 2014). We present two avenues for achieving pre-visual detection of drought stress using spectroscopy: the use of PLS-DA to detect drought directly from hyperspectral data based on a trained model, and the use of PLSR-derived predicted metabolic traits to detect drought through a trait-focused LDA (Figs 5–7), that allows for the elucidation of known response mechanisms in plants. The use of a trait-based approach requires the initial development of PLSR models using observed biochemical data for traits of interest, yet has the advantage of bringing specific

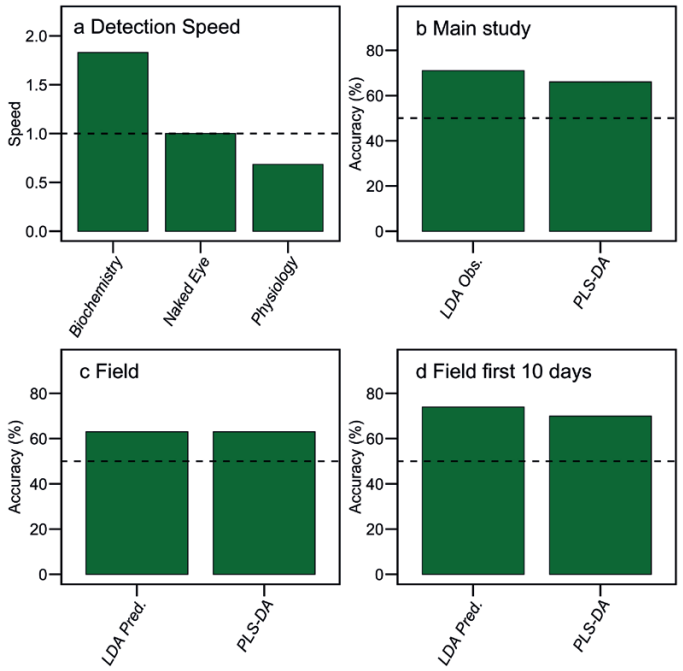

Fig. 7. Successful prediction of the class 'droughted' or 'watered' using spectra may be achieved using PLS-DA or a combination of PLSR and LDA. (A) Best-case scenarios of the speed of drought detection using biochemistry (Fig. 4) and physiology (Fig. 2) relative to detection using the naked eye show that only metabolic traits are sufficient for early detection, but these may be predicted using spectra; (B) prediction accuracy of drought or watered conditions using observed biochemical traits in an LDA model and using raw spectra in a PLS-DA model for plants in the main study; (C) prediction accuracy of drought or watered conditions using PLSR-predicted biochemical traits in an LDA model and using raw spectra in a PLS-DA model for field-grown *C. pepo*; (D) prediction accuracy of drought or watered conditions using PLSR-predicted biochemical traits in an LDA model and using spectra in a PLS-DA model for field-grown *C. pepo* during the first 10 d of drought.

predictions about trait values which may be of great importance in a plant breeding context. Moreover, once the model is developed, estimation of these traits in new leaves only requires the measurement of leaf reflectance (e.g. Serbin *et al.*, 2019), meaning that this approach provides a means for rapid trait evaluation in plants. The PLS-DA approach using raw spectra requires no initial biochemical data collection, leading to an increased speed and reduced cost; however, whilst more comprehensive than a two-band spectral index, it inherently provides less information about the metabolic status of the plants and requires a training dataset of spectra associated with known treatments.

Remote sensing techniques have been used to examine drought stress in the past, providing the advantage of being rapid, high-throughput, and non-destructive compared with traditional physiological and biochemical tools for measuring drought. However, drought stress detection using remote sensing has typically focused on spectral indices (Behmann *et al.*, 2014; Becker and Schmidhalter, 2017; Sun *et al.*, 2019). Computational approaches have also been used to analyse the full-spectrum data of hyperspectral images, expanding upon the utility of indices, yet without employing a mechanistic or trait-based approach (Römer *et al.*, 2012; Asaari *et al.*, 2019). Our study moves beyond the use of more traditional spectral vegetation indices to detect water status to provide quantitative links between spectral signatures and the underlying physiological changes that alter leaf reflectance (e.g. Fig. 5B). It also builds on and advances the demonstrated use of hyperspectral data for pre-visual detection of drought stress (Bayat *et al.*, 2016) and the quantitative relationships between spectra and leaf traits in crop plants (Yendrek *et al.*, 2017; Silva-Perez *et al.*, 2018; Ely *et al.*, 2019). Here we expand upon these previous examples by allowing for the attribution of the drought response to its underlying physiological traits, facilitating pre-visual detection of drought stress by predicting the values of known traits which change within the leaf before drought can be seen using the naked eye. This enables the integration of different approaches to provide greater insight into the drought response. Identifying key metabolic indicators of drought stress in the first instance but then applying spectroscopy techniques to predict these indicators throughout a crop breeding programme or growing season offers a much more efficient system for pre-visual and real-time measurement of plant stress. Moreover, in contrast to biochemical data reliant upon harvests followed by post-hoc analysis, spectral data can be collected and analysed in a continuous manner throughout an experiment, further increasing the power of this technique for detecting an effect.

Although physiological changes form an important and well-known part of the drought response, in the present study we did not observe a physiological change before drought was visible to the naked eye. The isohydric and anisohydric strategies of different plants (i.e. whether plants maintain water potential or tolerate a decrease in water potential under drought stress) form an additional consideration when examining stress responses (Tardieu *et al.*, 1996; Tardieu and Simonneau, 1998; McDowell *et al.*, 2008). Plants which tolerate a decrease in water potential, such as *H. annuus*, show a smaller decrease in photosynthesis under drought conditions, making gas exchange measurements a less effective means of detecting drought stress than in isohydric species, demonstrated in our study by the maintenance of photosynthesis in *H. annuus* up until the end of the experiment (Fig. 2), although we found that no species showed a pre-visual change in either A or g_{sw}.

In contrast to our physiological data, biochemical data revealed significant differences in advance of visual detection of drought (Fig. 7A), which is a key novel finding from this study. We observed an increase in ABA in all six species and an increase in proline in four species under drought conditions (Fig. 3), while sugars (glucose, fructose, and sucrose) were not a major driver of the drought response in our study. Leaf starch often decreases under drought stress, in line with lowered photosynthetic capacity (Thalmann and Santelia, 2017), and this was the

case for all six crops examined here (Fig. 3). The novel relationships we have shown between observed and predicted levels of ABA and proline (Fig. 5D, F) demonstrate an exciting potential for the non-destructive estimation of key drought stress metabolites, which we believe may be extrapolated to further phytohormones and signalling molecules that are central, early components of plant responses to a wide range of abiotic and biotic stresses (Claeys and Inzé, 2013).

For most traits, our PLSR models showed high accuracy and low error (Fig. 5). However, when comparing the models, the performance of the ABA model was lower, with an RMSE 19% of the observed data range for ABA, compared with RMSEs between 7% and 14% of the observed data range for the other traits (Fig. 5). Despite this, we believe that our findings represent a promising potential tool for drought detection for the suite of traits presented here. In particular, further research and additional datasets will probably improve the generality of the models (e.g. Serbin *et al.*, 2019), including for ABA, particularly if a broader range of data can be included in the model training. Furthermore, it should be noted that the validation plots presented in Fig. 5 are the results of an independent PLSR model validation, which provides a more accurate yet more conservative indication of model performance compared with the cross-validation approach used in many other studies (see Serbin *et al.*, 2014).

Our PLS-DA model results are comparable with those of previous studies which have demonstrated predictive capabilities with ~20 components in several models (Cavender-Bares *et al.*, 2016; Fallon *et al.*, 2020), and in one instance 34 components for a prediction accuracy of 61% (Fallon *et al.*, 2020). Although metabolic profiles under drought stress varied between the different species in our study, and the performance of the PLSR models differed between traits, the overall capacity for drought prediction using traits and spectra was substantial. In order to maximize trait variation and demonstrate a robust multispecies approach, we intentionally incorporated a range of crop species including: woody and herbaceous, graminoid and broadleaf, C_3 and C_4, temperate and arid, and crops grown for their wood, grain, or fruits. Whilst we advocate such an approach for developing an applicable model, we acknowledge that a species- or system-targeted approach could prove even more beneficial for making early predictions of drought stress in the breeding context if multiple cultivars of a single species are under examination.

The techniques we present here will impact crop breeding for water use efficiency and crop management, particularly in water-scarce areas. More research will be needed to fully elucidate the utility of our approach, since our multispecies approach was limited to only a small selection of agriculturally relevant species. In future work, it will be informative to expand the field system to a wider range of species and indeed a wider range of conditions, including additional abiotic and biotic stresses threatening crop production (Claeys and Inzé, 2013). Our approach will be particularly valuable for measurements of biotic stresses, which frequently have no externally measurable indicators, as well as for building upon pre-visual detection of visible stresses such as pathogen damage (Gold *et al.*, 2020). Future research should investigate the applicability of our approach for detecting a broader range of stresses, including combinations of stresses. It will also be important to broaden our technique to a range of genotypes within each species, in order to see if hyperspectral reflectance can detect differences in water stress across crop varieties, to fully realize the breeding potential of our approach. We further envisage the development of our technique in future experiments to encompass canopy- and field-scale spectroscopy utilizing existing gantry- and unoccupied aerial system (UAS)-mounted instruments (Smith *et al.*, 2002; Asner and Martin, 2008; Kokaly *et al.*, 2009; Virlet *et al.*, 2017; Coops *et al.*, 2019; Furbank *et al.*, 2019; Gerhards *et al.*, 2019; Shiklomanov *et al.*, 2019; Herrmann *et al.*, 2020; Meacham-Hensold *et al.*, 2020; Yang *et al.*, 2020; Burnett *et al.*, 2021). In future, these systems may be used with the novel inclusion of a multitrait prediction system to quantify complex characteristics such as the drought response at the metabolic level prior to visual detection. Our approach is more effective than one focused on individual metabolites, or a combination of atomic elements (Kunz *et al.*, 2017), due to the intricate nature of the plant metabolic response to drought (Claeys and Inzé, 2013). At the largest scale, successful development and adoption of these predictive techniques using satellite data would contribute additional detail to early warning systems for drought events across the globe (Sutanto *et al.*, 2019), impacting humanitarian relief and development work as well as ecosystem-level risk analyses to protect nature and agriculture against drought.

Supplementary data

The following supplementary data are available at *JXB* online.

Fig. S1. Example workflow for visual identification of drought.
Fig. S2. ROC analysis for LDA models.
Fig. S3. ROC analysis for PLS-DA models.

Acknowledgements

This work was supported by the United States Department of Energy contract no. DE-SC0012704 to Brookhaven National Laboratory. We thank A. Brinton, M.J.B. Burnett, E. O'Connor, G. Hilles, K. Scanlon, and D. Yang for assisting with data collection in the glasshouse; D. Anderson, S. Drew, C. Hamilton, B. Miller, and I. Rodriguez-Torres for assisting with data collection in the field; and K. Lewin and J. Anderson of Brookhaven National Laboratory for assistance with field and glasshouse management. We acknowledge J. Kim of Korea University for sharing the ABA extraction protocol, and M. Lundgren of Lancaster University for advice on LDA analysis.

Author contributions

ACB, SPS, KSE, and AR: experimental design; ACB and KD: data collection; ACB, SPS, KSE, AR, and KD: data analysis. ACB wrote the manuscript with contributions from all authors.

Data availability

The full raw dataset accompanying this manuscript is available online at EcoSIS (ecosis.org) at https://doi.org/10.21232/UTK8zaW4.

References

AghaKouchak A, Farahmand A, Melton F, Teixeira J, Anderson M, Wardlow B, Hain C. 2015. Remote sensing of drought: progress, challenges and opportunities. Reviews of Geophysics **53**, 452–480.

Araus JL, Cairns JE. 2014. Field high-throughput phenotyping: the new crop breeding frontier. Trends in Plant Science **19**, 52–61.

Araus JL, Kefauver SC, Zaman-Allah M, Olsen MS, Cairns JE. 2018. Translating high-throughput phenotyping into genetic gain. Trends in Plant Science **23**, 451–466.

Asaari MSM, Mertens S, Dhondt S, Inzé I, Wuyts N, Scheunders P. 2019. Analysis of hyperspectral images for detection of drought stress and T recovery in maize plants in a high-throughput phenotyping platform. Computers and Electronics in Agriculture **162**, 749–758.

Asner GP, Martin RE. 2008. Spectral and chemical analysis of tropical forests: scaling from leaf to canopy levels. Remote Sensing of Environment **112**, 3958–3970.

Ballester C, Zarco-Tejada PJ, Nicolás E, Alarcón JJ, Fereres E, Intrigliolo DS, Gonzalez-Dugo V. 2018. Evaluating the performance of xanthophyll, chlorophyll and structure-sensitive spectral indices to detect water stress in five fruit tree species. Precision Agriculture **19**, 178–193.

Bayat B, Van der Tol C, Verhoef W. 2016. Remote sensing of grass response to drought stress using spectroscopic techniques and canopy reflectance model inversion. Remote Sensing **8**, 557.

Becker E, Schmidhalter U. 2017. Evaluation of yield and drought using active and passive spectral sensing systems at the reproductive stage in wheat. Frontiers in Plant Science **8**, 379.

Behmann J, Steinrücken J, Plümer L. 2014. Detection of early plant stress responses in hyperspectral images. ISPRS Journal of Photogrammetry and Remote Sensing **93**, 98–111.

Burnett AC, Anderson J, Davidson KJ, *et al*. 2021. A best-practice guide to predicting plant traits from leaf-level hyperspectral data using partial least squares regression. Journal of Experimental Botany. doi:1093/jxb/erab295.

Burnett AC, Davidson KJ, Serbin SP, Rogers A. 2019. The 'one-point method' for estimating maximum carboxylation capacity of photosynthesis: a cautionary tale. Plant, Cell & Environment **42**, 2472–2481.

Burnett AC, Rogers A, Rees M, Osborne CP. 2016. Carbon source–sink limitations differ between two species with contrasting growth strategies. Plant, Cell & Environment **39**, 2460–2472.

Burnett AC, Rogers A, Rees M, Osborne CP. 2018. Nutrient sink limitation constrains growth in two barley species with contrasting growth strategies. Plant Direct **2**, e00094.

Burnett AC, Serbin SP, Rogers A. 2021. Source:sink imbalance detected with leaf- and canopy-level spectroscopy in a field-grown crop. Plant, Cell and Environment. doi:10.1111/pce.14056.

Cattivelli L, Rizza F, Badeck FW, Mazzucotelli E, Mastrangelo AM, Francia E, Marè C, Tondelli A, Stanca AM. 2008. Drought tolerance improvement in crop plants: an integrated view from breeding to genomics. Field Crops Research **105**, 1–14.

Cavender-Bares J, Meireles JE, Couture JJ, *et al.* 2016. Associations of leaf spectra with genetic and phylogenetic variation in oaks: prospects for remote detection of biodiversity. Remote Sensing **8**, 221.

Chaves MM, Flexas J, Pinheiro C. 2009. Photosynthesis under drought and salt stress: regulation mechanisms from whole plant to cell. Annals of Botany **103**, 551–560.

Claeys H, Inzé D. 2013. The agony of choice: how plants balance growth and survival under water-limiting conditions. Plant Physiology **162**, 1768–1779.

Coops NC, Goodbody TRH, Cao L. 2019. Four steps to extend drone use in research. Nature **572**, 433–435.

Cotrozzi L, Couture JJ. 2020. Hyperspectral assessment of plant responses to multi-stress environments: prospects for managing protected agrosystems. Plants, People, Planet **2**, 244–258.

Couture J, Singh A, Rubert-Nason K, Serbin S, Lindroth R, Townsend P. 2016. Spectroscopic determination of ecologically relevant plant secondary metabolites. Methods in Ecology and Evolution **7**, 1402–1412.

Ely KS, Burnett AC, Lieberman-Cribbin W, Serbin SP, Rogers A. 2019. Spectroscopy can predict key leaf traits associated with source–sink balance and carbon–nitrogen status. Journal of Experimental Botany **70**, 1789–1799.

Ely KS, Rogers A, Agarwal DA, *et al.* 2021. A reporting format for leaf-level gas exchange data and metadata. Ecological Informatics **61**, 101232.

Erickson R, Michelini F. 1957. The plastochron index. American Journal of Botany **44**, 297–305.

Fàbregas N, Fernie AR. 2019. The metabolic response to drought. Journal of Experimental Botany **70**, 1077–1085.

Fallon B, Yang A, Lapadat C, Armour I, Juzwik J, Montgomery RA, Cavender-Bares J. 2020. Spectral differentiation of oak wilt from foliar fungal disease and drought is correlated with physiological changes. Tree Physiology **40**, 377–390.

FAO. 2018. The future of food and agriculture. Alternative pathways to 2050. Rome: FAO.

Franklin J, Serra-Diaz JM, Syphard AD, Regan HM. 2016. Global change and terrestrial plant community dynamics. Proceedings of the National Academy of Sciences, USA **113**, 3725–3734.

Furbank RT, Jimenez-Berni JA, George-Jaeggli B, Potgieter AB, Deery DM. 2019. Field crop phenomics: enabling breeding for radiation use efficiency and biomass in cereal crops. New Phytologist **223**, 1714–1727.

Gerhards M, Schlerf M, Mallick K, Udelhoven T. 2019. Challenges and future perspectives of multi-/hyperspectral thermal infrared remote sensing for crop water-stress detection: a review. Remote Sensing **11**, 1240.

Gold KM, Townsend PA, Chlus A, Herrmann I, Couture JJ, Larson ER, Gevens AJ. 2020. Hyperspectral measurements enable pre-symptomatic detection and differentiation of contrasting physiological effects of late blight and early blight in potato. Remote Sensing **12**, 286.

Herrmann I, Bdolach E, Montekyo Y, Rachmilevitch S, Townsend PA, Karnieli A. 2020. Assessment of maize yield and phenology by drone-mounted superspectral camera. Precision Agriculture **21**, 51–76.

Kim J, Malladi A, van Iersel MW. 2012. Physiological and molecular responses to drought in Petunia: the importance of stress severity. Journal of Experimental Botany **63**, 6335–6345.

Kokaly RF, Asner GP, Ollinger SV, Martin ME, Wessman CA. 2009. Characterizing canopy biochemistry from imaging spectroscopy and its application to ecosystem studies. Remote Sensing of Environment **113**, S78–S91.

Kuhn M. 2008. Building predictive models in R using the caret package. Journal of Statistical Software **28**, 1–26.

Kunz JN, Voronine DV, Lee HW, Sokolov AV, Scully MO. 2017. Rapid detection of drought stress in plants using femtosecond laser-induced breakdown spectroscopy. Optics Express **25**, 7251–7262.

Leakey ADB, Ferguson JN, Pignon CP, Wu A, Jin Z, Hammer GL, Lobell DB. 2019. Water use efficiency as a constraint and target for improving the resilience and productivity of C_3 and C_4 crops. Annual Review of Plant Biology **70**, 781–808.

McDowell N, Pockman WT, Allen CD, *et al.* 2008. Mechanisms of plant survival and mortality during drought: why do some plants survive while others succumb to drought? New Phytologist **178**, 719–739.

Meacham-Hensold K, Fu P, Wu J, *et al.* 2020. Plot-level rapid screening for photosynthetic parameters using proximal hyperspectral imaging. Journal of Experimental Botany **71**, 2312–2328.

Meacham-Hensold K, Montes CM, Wu J, *et al.* 2019. High-throughput field phenotyping using hyperspectral reflectance and partial least squares regression (PLSR) reveals genetic modifications to photosynthetic capacity. Remote Sensing of Environment **231**, 111176.

Mevik B, Wehrens R. 2007. The pls package: principal component and partial least squares regression in R. Journal of Statistical Software **18**, 1–23.

Morison JI, Baker NR, Mullineaux PM, Davies WJ. 2008. Improving water use in crop production. Philosophical Transactions of the Royal Society B: Biological Sciences **363**, 639–658.

Munemasa S, Hauser F, Park J, Waadt R, Brandt B, Schroeder JI. 2015. Mechanisms of abscisic acid-mediated control of stomatal aperture. Current Opinion in Plant Biology **28**, 154–162.

Ort DR, Merchant SS, Alric J, *et al.* 2015. Redesigning photosynthesis to sustainably meet global food and bioenergy demand. Proceedings of the National Academy of Sciences, USA **112**, 8529–8536.

Poore J, Nemecek T. 2018. Reducing food's environmental impacts through producers and consumers. Science **360**, 987–992.

Poorter H, Fiorani F, Pieruschka R, Wojciechowski T, van der Putten WH, Kleyer M, Schurr U, Postma J. 2016. Pampered inside, pestered outside? Differences and similarities between plants growing in controlled conditions and in the field. New Phytologist **212**, 838–855.

Poorter H, Fiorani F, Stitt M, *et al.* 2012. The art of growing plants for experimental purposes: a practical guide for the plant biologist. Functional Plant Biology **39**, 821–838.

R Core Team. 2019. R: a language and environment for statistical computing. Vienna, Austria: R Foundation for Statistical Computing.

Rapaport T, Hochberg U, Cochavi A, Karnieli A, Rachmilevitch S. 2017. The potential of the spectral 'water balance index' (WABI) for crop irrigation scheduling. New Phytologist **216**, 741–757.

Reynolds M, Langridge P. 2016. Physiological breeding. Current Opinion in Plant Biology **31**, 162–171.

Römer C, Wahabzada M, Ballvora A, *et al.* 2012. Early drought stress detection in cereals: simplex volume maximisation for hyperspectral image analysis. Functional Plant Biology **39**, 878–890.

Rossini M, Fava F, Cogliati S, *et al.* 2013. Assessing canopy PRI from airborne imagery to map water stress in maize. ISPRS Journal of Photogrammetry and Remote Sensing **86**, 168–177.

Sah SK, Reddy KR, Li J. 2016. Abscisic acid and abiotic stress tolerance in crop plants. Frontiers in Plant Science **7**, 1–26.

Schweiger, AK. 2020. Spectral field campaigns: planning and data collection. In: Cavender-Bares J, Gamon JA, Townsend PA, eds. Remote sensing of plant biodiversity. Cham: Springer International Publishing, 385–423.

Serbin SP, Dillaway DN, Kruger EL, Townsend PA. 2012. Leaf optical properties reflect variation in photosynthetic metabolism and its sensitivity to temperature. Journal of Experimental Botany **63**, 489–502.

Serbin SP, Singh A, Desai AR, Dubois SG, Jablonski AD, Kingdon CC, Kruger EL, Townsend PA. 2015. Remotely estimating photosynthetic capacity, and its response to temperature, in vegetation canopies using imaging spectroscopy. Remote Sensing of Environment **167**, 78–87.

Serbin SP, Singh A, McNeil BE, Kingdon CC, Townsend PA. 2014. Spectroscopic determination of leaf morphological and biochemical traits for northern temperate and boreal tree species. Ecological Applications **24**, 1651–1669.

Serbin SP, Wu J, Ely KS, Kruger EL, Townsend PA, Meng R, Wolfe BT, Chlus A, Wang Z, Rogers A. 2019. From the Arctic to the tropics: multibiome prediction of leaf mass per area using leaf reflectance. New Phytologist **224**, 1557–1568.

Shiklomanov AN, Bradley BA, Dahlin KM, Fox AM, Gough CM, Hoffman FM, Middleton EM, Serbin SP, Smallman L, Smith WK. 2019. Enhancing global change experiments through integration of remote-sensing techniques. Frontiers in Ecology and the Environment **17**, 215–224.

Silva-Perez V, Molero G, Serbin SP, Condon AG, Reynolds MP, Furbank RT, Evans JR. 2018. Hyperspectral reflectance as a tool to measure biochemical and physiological traits in wheat. Journal of Experimental Botany **69**, 483–496.

Simkin AJ, López-Calcagno PE, Raines CA. 2019. Feeding the world: improving photosynthetic efficiency for sustainable crop production. Journal of Experimental Botany **70**, 1119–1140.

Smith ML, Ollinger SV, Martin ME, Aber JD, Hallett RA, Goodale CL. 2002. Direct estimation of aboveground forest productivity through hyperspectral remote sensing of canopy nitrogen. Ecological Applications **12**, 1286–1302.

Sreenivasulu N, Harshavardhan VT, Govind G, Seiler C, Kohli A. 2012. Contrapuntal role of ABA: does it mediate stress tolerance or plant growth retardation under long-term drought stress? Gene **506**, 265–273.

Sun H, Feng M, Xiao L, Yang W, Wang C, Jia X, Zhao Y, Zhao C, Muhammad SK, Li D. 2019. Assessment of plant water status in winter wheat (*Triticum aestivum* L.) based on canopy spectral indices. PLoS One **14**, e0216890.

Sunkar R, ed. 2010. Plant stress tolerance: methods and protocols. Cham: Springer.

Susič N, Žibrat U, Širca S, Strajnar P, Razinger J, Knapič M, Vončina A, Urek G, Stare BG. 2018. Discrimination between abiotic and biotic drought stress in tomatoes using hyperspectral imaging. Sensors & Actuators B **273**, 842–852.

Sutanto SJ, van der Weert M, Wanders N, Blauhut V, Van Lanen HAJ. 2019. Moving from drought hazard to impact forecasts. Nature Communications **10**, 1–7.

Tardieu F, Lafarge T, Simonneau T. 1996. Stomatal control by fed or endogenous xylem ABA in sunflower: interpretation of correlations between leaf water potential and stomatal conductance in anisohydric species. Plant, Cell & Environment **19**, 75–84.

Tardieu F, Simonneau T. 1998. Variability among species of stomatal control under fluctuating soil water status and evaporative demand: modelling isohydric and anisohydric behaviours. Journal of Experimental Botany **49**, 419–432.

Thalmann M, Santelia D. 2017. Starch as a determinant of plant fitness under abiotic stress. New Phytologist **214**, 943–951.

Virlet N, Sabermanesh K, Sadeghi-Tehran P, Hawkesford MJ. 2017. Field Scanalyzer: an automated robotic field phenotyping platform for detailed crop monitoring. Functional Plant Biology **44**, 143–153.

Wold S, Sjöström M, Eriksson L. 2001. PLS-regression: a basic tool of chemometrics. Chemometrics and Intelligent Laboratory Systems **58**, 109–130.

Yang D, Meng R, Morrison BD, McMahon A, Hantson W, Hayes DJ, Breen AL, Salmon VG, Serbin SP. 2020. A multi-sensor unoccupied aerial system improves characterization of vegetation composition and canopy properties in the Arctic tundra. Remote Sensing **12**, 2638.

Yendrek CR, Tomaz T, Montes CM, Cao Y, Morse AM, Brown PJ, McIntyre LM, Leakey AD, Ainsworth EA. 2017. High-throughput phenotyping of maize leaf physiological and biochemical traits using hyperspectral reflectance. Plant Physiology **173**, 614–626.

Zarco-Tejada PJ, González-Dugo V, Berni JAJ. 2012. Fluorescence, temperature and narrow-band indices acquired from a UAV platform for water stress detection using a micro-hyperspectral imager and a thermal camera. Remote Sensing of Environment **117**, 322–337.

Zarco-Tejada PJ, González-Dugo V, Williams LE, Suárez L, Berni JAJ, Goldhamer D, Fereres E. 2013. A PRI-based water stress index combining structural and chlorophyll effects: assessment using diurnal narrow-band airborne imagery and the CWSI thermal index. Remote Sensing of Environment **138**, 38–50.

Zhu JK. 2016. Abiotic stress signaling and responses in plants. Cell **167**, 313–324.

Zovko M, Žibrat U, Knapič M, Kovačić MB, Romić D. 2019. Hyperspectral remote sensing of grapevine drought stress. Precision Agriculture **20**, 325–347.